STAFF SUMMARY SHEET

	TO	ACTION	SIGNATURE (Surname), GRADE AND DATE		TO	ACTION	SIGNATURE (Surname), GRADE AND DATE
1	DFP	sig	GAUTHIER, LtCol, 18Nov14	6			
2	DFER	approve	SOLTI, AD25, 18 Nov 14	7			
3	DFP	action		8			
4				9			
5				10			

SURNAME OF ACTION OFFICER AND GRADE	SYMBOL	PHONE	TYPIST'S INITIALS	SUSPENSE DATE
Gauthier, O-5	DFP	333-4345	bgw	20141120

SUBJECT		DATE
Clearance of Matierial for Public Release	USAFA-DF-PA/ 501	20141118

SUMMARY

1. PURPOSE. To provide security and policy review on the document at Tab 1 prior to release to the public.

2. BACKGROUND.
Authors: Benjamin G. Ward (DFP, 719-271-6748)

Title: Maximizing power output from continuous-wave single-frequency fiber amplifiers

Document Type: Journal Article

Description: This is an article describing the optimization of fiber amplifiers subject to stimulated Brillouin scattering and stimulated thermal Rayleigh scattering.

Release Information: The manuscript will be submitted to the journal Optics Letters.

Recommended distribution statement: Distribution A, Approved for public release, distribution unlimited.

3. DISCUSSION. Lt. Col. Benjamin Ward is a former faculty member who continues to publish research work on high performance modeling and simulation of fiber lasers and amplifiers. I am submitting this public release document on his behalf.

4. RECOMMENDATION. Sign coord block above indicating document is suitable for public release. Suitability is based solely on the document being unclassified, not jeopardizing DoD interests, and accurately portraying official policy.

//signed//
MICHAEL L. GAUTHIER, Lt Col, USAF
Deputy Head for Research,
Department of Physics

Tabs
1. Article

Maximizing power output from continuous-wave single-frequency fiber amplifiers

Benjamin G. Ward,[1,*]

[1]*Physics Department, United States Air Force Academy, 2354 Fairchild Dr. Ste. 2A31, USAF Academy, CO 80840, USA*
**Corresponding author: benjamin.ward.1@us.af.mil*

Received Month X, XXXX; revised Month X, XXXX; accepted Month X, XXXX; posted Month X, XXXX (Doc. ID XXXXX); published Month X, XXXX

This letter reports on a method of maximizing the power output from highly saturated cladding-pumped continuous-wave single-frequency fiber amplifiers simultaneously taking into account the stimulated Brillouin scattering and transverse modal instability thresholds. This results in a design figure of merit depending on the fundamental mode overlap with the doping profile, the peak Brillouin gain coefficient, and the peak mode coupling gain coefficient. This figure of merit is then numerically analyzed for three candidate fiber designs including standard, segmented acoustically tailored, and micro segmented acoustically tailored photonic crystal fibers. It is found that each of the latter two fibers should enable a 50% higher output power than standard photonic crystal fiber. © 2014 Optical Society of America

OCIS Codes: (140.3510) Lasers, fiber, (140.3280) Laser amplifiers, (060.2280) Fiber design and fabrication, (190.5890) Scattering, stimulated, (190.3100) Instabilities and chaos.
http://dx.doi.org/10.1364/OL.99.099999

High-power continuous-wave single frequency sources are important for metrological applications such as gravitational interferometry [1], coherent laser radar [2], and non-linear conversion [3]. The maximum power achievable with single frequency fiber amplifiers is limited either by stimulated Brillouin scattering (SBS) or thermal modal instability. Recently, a single frequency fiber amplifier with an SBS-limited output power of 811 Watts was demonstrated using a photonic crystal fiber with gain and segmented acoustic tailoring (SAT) [4]. The gain tailoring of this fiber primarily served to mitigate transverse modal instability while the acoustic tailoring, together with a longitudinal thermal gradient, served to mitigate SBS. The acoustic tailoring was devised in order to distribute the mode field intensity approximately evenly over regions of differing acoustic velocities in order to reduce the effective peak Brillouin gain coefficient. It has been shown theoretically that there is an optimal acoustic domain size for SBS suppression in thermally uniform fibers that exploits elastic coupling between reduced-size acoustic domains to suppress the resonant electrostrictive response resulting in a smaller peak Brillouin gain coefficient [5].

A sizeable amount of evidence has been presented that suggests the fundamental mechanism leading to modal instability is Stimulated Thermal Rayleigh Scattering (STRS) [6]. The SBS and STRS processes share several key aspects in common. They both can be described as the scattering of one mode into another due to a non-linear refractive index response to the intensity interference pattern of the two modes. In the case of SBS the modes are separated from each other the ~16 GHz Stokes shift and power may be scattered between the same or different transverse modes while in the case of STRS the modes are separated by a frequency offset typically of the order of kHz and the power is scattered between different transverse modes. In the case of SBS the index disturbance is caused by electrostriction while for STRS it is caused by the thermo-optic effect. For most non-linear processes, increasing the mode field area increases the threshold. The STRS the threshold on the other hand decreases with increasing mode field area in most cases as will be shown below. This sets up a situation wherein design principles for increasing the STRS threshold oppose those for increasing the threshold of SBS as well as most other parasitic nonlinearities. The maximum combined threshold for single-frequency systems such as those considered here may then be achieved at the design point where the SBS and STRS thresholds coincide.

This letter begins with a derivation of the conditions for maximum output power from a single-frequency fiber amplifier subject to SBS and STRS, followed by analysis of example fiber designs, and the conclusion.

The SBS threshold power is given by [7]

$$P_{\mathrm{SBS}} = \frac{C_{SBS} A_{\mathrm{eff}}}{g_B L_{\mathrm{eff,SBS}}} \qquad (1)$$

where A_{eff} is the non-linear effective mode area, g_B is the Brillouin gain coefficient, $L_{\mathrm{eff,SBS}}$ is the effective fiber length for SBS, and C_{SBS} is a dimensionless constant of approximate value 10-20 depending on seeding conditions for the backward-propagating Stokes wave and the definition of the SBS threshold.

In order for (1) to be useful it is necessary to impose a condition on total pump absorption to ensure adequate optical efficiency

$$C_{\mathrm{abs}} = \Gamma_1 N_1 L_{\mathrm{eff,SBS}} \frac{A_{\mathrm{eff}}}{A_{\mathrm{clad}}} \qquad (2)$$

where $N_1 \equiv N_{\mathrm{ion}} \sigma_{\mathrm{ap}}$ for a highly saturated amplifier and where A_{clad} is the pump cladding area, A_{eff} is the doped

core area, Γ_1 is the overlap fraction of the fundamental mode with the doped core area,

$$\Gamma_1 \equiv \iint_{A_d} \left|\psi_1(\vec{r})\right|^2 d^2\vec{r} \qquad (3)$$

and N_{ion} is the doping concentration which leads to the following value for the SBS threshold

$$P_{\text{SBS}} = \frac{C_{SBS}\Gamma_1 N_{\text{ion}}\sigma_{\text{ap}}A_{\text{eff}}^2}{C_{\text{abs}}g_B A_{\text{clad}}} \qquad (4)$$

Thanks to a recently published expression for the modal power transferred in an amplifier due to STRS [8], an expression may be derived in a similar fashion for the STRS threshold in a well-saturated amplifier. The power transferred through the STRS process into a higher order mode at a single shifted frequency is given by

$$P_2(L) = P_{2,0}(L)\exp\left[\chi_0\int_0^L \frac{\tilde{g}^2(z)}{g_0(z)}P_1(z)dz\right] \qquad (5)$$

where $P_{2,0}(L)$ is the output power in the higher order mode in the absence of inter-modal coupling, χ_0 is the STRS mode coupling coefficient [7], $\tilde{g}$ is the effective saturated signal gain, g_0 is the small signal gain, and $P_1(z)$ is the power in the fundamental mode. Borrowing the methodology from the SBS case, the threshold condition is reached when the term in the exponential reaches a suitably high value. Counter-pumped amplifiers exhibit more uniform saturation profiles than co-pumped amplifiers due to the similar behavior with length of the pump and signal intensities. In the case of a highly-saturated counter-pumped amplifier the approximation

$$P_1(z) \approx \frac{\lambda_p}{\lambda_s}P_p(z) \qquad (6)$$

is very useful. This approximation is fairly accurate if the residual pump power is comparable to the seed power, a condition not uncommon experimentally. The saturated gain is given by

$$\tilde{g} = N_{\text{ion}}\left(\frac{\sigma_{es}\sigma_{ap}}{\sigma_{ap}+\sigma_{ep}}\right)\Bigg/\left(1+\frac{\Gamma_1 P_1 A_{\text{clad}} I_{\text{p,sat}}}{P_p A_d I_{\text{s,sat}}}\right) \qquad (7)$$

from which the highly-saturated and small-signal limits may be derived leading to the following approximate expression for the STRS threshold power

$$P_{\text{STRS}} = \frac{C_{STRS}}{\tilde{\sigma}N_{\text{ion}}\chi_0 L_{\text{eff,STRS}}}\left(\frac{\lambda_p\Gamma_1 A_{\text{clad}}}{\lambda_s A_d}\right)^2 \qquad (8)$$

where A_{clad} is the pump cladding area, A_d is the doped core area, Γ_1 is the overlap fraction of the fundamental mode with the doped core area, N_{ion} is the doping concentration, χ_0 is the STRS mode coupling coefficient, $L_{\text{eff,STRS}}$ is the STRS effective length (which may differ slightly from the SBS effective length), C_{STRS} is the STRS dimensionless constant, and $\tilde{\sigma}$ is a combination of cross-sections given by

$$\tilde{\sigma} \equiv \frac{\sigma_{es}\sigma_{ap}\left(\sigma_{ap}+\sigma_{ep}\right)}{\left(\sigma_{as}+\sigma_{es}\right)^2} \qquad (9)$$

where the subscripts e and a denote emission and absorption while s and p denote signal and pump. The threshold coefficient C_{STRS} can be expected to differ depending on the particular characteristics of the amplifier under consideration nevertheless the threshold dependencies given in (8) should be useful for optimizing fiber amplifier designs and configurations. Once again imposing the pump absorption constraint and using the approximation $A_d = \Gamma_1 A_{\text{eff}}$ leads to

$$P_{\text{STRS}} = \frac{C_{STRS}\Gamma_1\sigma_{\text{ap}}A_{\text{clad}}}{C'_{\text{abs}}\tilde{\sigma}\chi_0 A_{\text{eff}}}\left(\frac{\lambda_p}{\lambda_s}\right)^2 \qquad (10)$$

Comparing (4) and (10) it is immediately evident that increasing the mode field area increases the SBS threshold but decreases the STRS threshold. If modal area is chosen as the independent fiber design parameter, then setting the STRS and SBS thresholds equal yields an optimal cladding area and maximum attainable output power. The optimal cladding area is given by

$$A_{\text{clad}} = \left[A_{\text{eff}}^3\frac{C'_{\text{abs}}C_{SBS}N_{\text{ion}}\tilde{\sigma}\chi_0}{C_{STRS}C_{\text{abs}}g_B}\left(\frac{\lambda_s}{\lambda_p}\right)^2\right]^{1/2}. \qquad (11)$$

It is very interesting to note that the optimal cladding area depends on the SBS or STRS-suppressing properties of the core design as reflected in the values of g_B and χ_0. Substitution of (11) into either (4) or (10) yields the maximum power.

$$P_{\text{max}} \approx \Gamma_1\sigma_{\text{ap}}\frac{\lambda_p}{\lambda_s}\left[\frac{C_{SBS}C_{STRS}}{C_{\text{abs}}C'_{\text{abs}}}\frac{N_{\text{ion}}A_{\text{eff}}}{\tilde{\sigma}g_B\chi_0}\right]^{1/2} \qquad (12)$$

Thus the prescription for maximum power is to make the mode field area as large as possible, and then set the cladding size to the optimum value. The dependencies in (12) are very intuitive. For given material parameters, the maximum power may be increased by increasing the fundamental mode overlap fraction, decreasing the maximum value of the Brillouin gain coefficient, and decreasing the maximum value of the mode coupling coefficient. Equation (12) is not expected to yield precise values due to the uncertainties present in the numerous parameters therein. Furthermore, the experimental determination of these parameters is beyond the scope of this work. Rather, this expression may be used to compare candidate fiber designs with tailored doping and acoustic profiles with respect to power scaling potential.

One successfully demonstrated method of profile tailoring is the microstructuring of the core whereby the core design is constructed of pixels of different material compositions in a prescribed geometric arrangement [4]. A given set of finite materials constrains the power optimization using (12). For the purposes of comparing waveguide design approaches, it is convenient to use the material set previously employed [4] consisting of pure

fused silica and two varieties of aluminum, germanium, fluorine and ytterbium-doped fused silica. The present aim is then to assess the power scaling potential of different arrangements of pixels in the core using this material system while keeping the other design parameters fixed. Under these constraints, the proper figure of merit derived from (12) is

$$F = \Gamma_1 \Big/ \sqrt{g_B \chi_0}. \tag{13}$$

Vectorial finite element techniques previously described have been used to calculate the fundamental mode overlap fraction and the peak Brillouin gain coefficient for the cases treated here [5,9]. Additionally, these have now been adapted to calculate the modal coupling constant χ_0 as will now be described.

Assuming harmonic time dependence, the frequency domain heat equation governing the temperature within the fiber is

$$i\Omega\rho C T(\vec{r}_\perp,\Omega) = \kappa\nabla^2 T(\vec{r}_\perp,\Omega) + Q(\vec{r}_\perp,\Omega) \tag{14}$$

as has been previously described [6,8] where ρ is the mass density, C is the heat capacity, κ is the thermal conductivity, T is the temperature, Q is the heating term, and Ω is frequency of a given harmonic component of the oscillating temperature. Invoking the finite element technique (14) begins the variational form governing the temperature behavior

$$\Im_\Omega = \iint_A \left[\frac{i\Omega\rho C}{2} \left| T(\vec{r}_\perp,\Omega) \right|^2 + \frac{\kappa}{2} \left| \nabla T(\vec{r}_\perp,\Omega) \right|^2 - Q(\vec{r}_\perp,\Omega) T(\vec{r}_\perp,\Omega) \right] d^2\vec{r}. \tag{15}$$

The temperature and heat distributions are then approximated by their values at the vertices of the same curvilinear triangular mesh used in the optical calculations and the area integral approximated as a sum of integrals over elements with locally uniform material properties leading to a linear system determining the frequency dependent temperature distribution

$$(i\Omega\rho C\mathbf{M} + \kappa\mathbf{K})\mathbf{T}_\Omega \equiv \mathbf{L}_\Omega \Delta\mathbf{T}_\Omega = \mathbf{Q}_\Omega. \tag{16}$$

Upon solving (16) for the temperature vector, the temperatures and mode field profiles may then be numerically integrated over the fiber cross-section to yield the frequency-dependent modal coupling coefficient

$$\chi_0(\Omega) \equiv \frac{dn}{dT} \frac{(1-\eta)k_0}{\kappa n_{\text{eff}}} \operatorname{Im}\left[\sum_{t=1}^{N_e} \psi_{1t}^* \psi_{2t} \Delta T_{t,\Omega} A_t \right] \tag{17}$$

where dn/dT is the thermo-optic coefficient, $(1-\eta)$ is the quantum defect fraction, k_0 is the vacuum wave vector, and n_{eff} is the fundamental modal index.

Using (13), three candidate fiber designs with different doping and acoustic profiles are assessed. The first of these has uniform doping throughout most of the core. The second is similar to the SAT fiber described previously [4], and the third uses a segmented acoustically tailored core but with smaller acoustic domains that is termed a micro-SAT design. In order to subdivide the core cells into smaller domains in the micro-SAT fiber design it is necessary to introduce a slight asymmetry into the lattice. For consistency of comparison, this arrangement is also maintained for the PCF and SAT fiber designs. All optical and mechanical properties of the fibers are the same as those given in prior works [5,10] except that the two varieties of Yb-doped glass are characterized by acoustic velocities of 5851 m/s and 5769 m/s and bulk Brillouin line widths of 45 MHz and 46 MHz but have the same Yb doping concentrations.

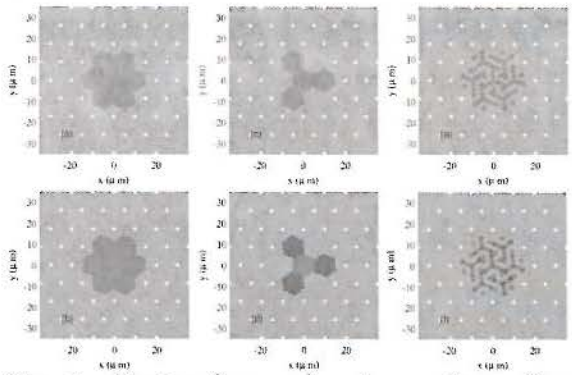

Fig. 1. Doping (top row) and acoustic profiles (bottom row) of a PCF (left), SAT (center) and μSAT (right) fibers. Darker shades of grey represent lower acoustic velocities whereas all doping concentrations are constant.

Fig. 1 depicts the acoustic and doping profiles of each fiber. These include the first baseline fiber design considered is a photonic crystal fiber (PCF) with an arrangement of seven uniform cells of doped material in the core taking the place of air holes in the photonic crystal lattice resulting in a doped area of 604 square micrometers. The lattice pitch is 10 micrometers with a hole diameter to pitch ratio of 0.17 resulting in a mode field diameter of 27 micrometers and a mode field area of 576 square micrometers.

The second fiber design considered is a SAT PCF with a design similar to one previously discussed [4]. This fiber has a center cell surrounded by alternating cells of lower velocity doped fused silica and un-doped fused silica. Each cell has an area of 86 square micrometers.

The third fiber design considered is a μSAT PCF with a new design. The acoustic domain size in this case is 2.1 micrometers, which is slightly larger than the optimal size determined previously for a randomly acoustically microstructured PCF [5]. In contrast to the random acoustic structure, the μSAT PCF has the domains arranged in a specified fashion. Each core cell is subdivided into 19 subcells. Within each cell there are 6 high-velocity subcells, 4 low-velocity subcells, and 9 un-doped subcells. This arrangement was determined through trial and error to yield the lowest predicted peak Brillouin gain coefficient. It is important to note that for acoustic domains this small, vectorial analysis is required to predict the Brillouin gain spectrum [5].

Figure 2 shows the calculated Brillouin gain spectra for the three fibers. The PCF exhibits a single large peak

near 15.94 GHz with a small residual peak at 16.28 GHz due to residual modal overlap with undoped regions at the core edge. The SAT PCF exhibits three well-defined peaks corresponding to the three acoustic velocities comprising the core at 15.73 GHz, 15.95 GHz, and 16.28 GHz. These three main peaks are also evident in the spectrum of the μSAT PCF, but they are slightly broadened and the two lower frequency peaks are upshifted in frequency.

Figure 3 shows the calculated Stimulated Thermal Rayleigh Scattering mode coupling gain spectra for the three fibers. The peak mode coupling gain occurs at a frequency shift of -3.1 kHz that is the same for all three fibers. The mode coupling gain profiles are nearly identical for the SAT and μSAT PCF.

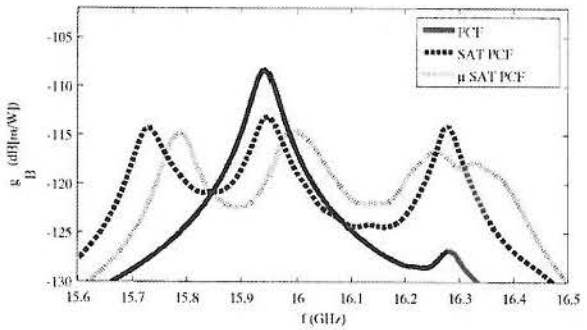

Fig. 2. Calculated Brillouin gain spectra of the three fibers

Table 1 presents the relevant amplifier performance parameters under the conditions described above. Both the SAT PCF and μSAT PCF exhibit an improvement of about 50% in maximum power over the PCF. Interestingly even though the μSAT PCF has an identical modal coupling constant to the SAT PCF as well as a lower peak Brillouin gain coefficient, its lower overlap fraction lowers its figure of merit below that of the SAT PCF. This shows that it is important to consider the overlap fraction of the fundamental mode with the doped core area when assessing the power scaling potential of a transverse waveguide design.

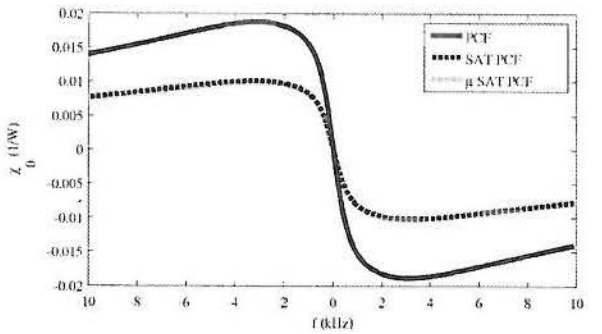

Fig. 3. Calculated mode coupling gain for the three fibers where $f = 2\pi\Omega$

Table 1. Amplifier Performance Parameters

Fiber Type	Γ_1	g_B[m/W]	χ_0[1/m]	F [W$^{1/2}$]
PCF	0.90	1.5×10^{-11}	0.019	1.7×10^{6}
SAT PCF	0.57	4.9×10^{-12}	0.010	2.6×10^{6}
μSAT PCF	0.47	3.5×10^{-12}	0.010	2.5×10^{6}

The results presented here show that maximizing the output power of single-frequency continuous wave fiber amplifiers requires considering simultaneously both the thermally-induced mode coupling gain as well as the Brillouin gain coefficient. Furthermore, the line of development presented here is applicable to other non-linearities that have thresholds that scale with the mode field area as the SBS threshold does. Due to gain saturation, the STRS threshold exhibits distinctly different behavior, notably a decrease as mode field area is increased for a given pump cladding size.

The author would like to acknowledge a grant of computational time from the DoD High Performance Computing Modernization Program, and funding support provided by the DoD High Energy Laser Joint Technology Office, and funded through the Army Research Office through grant 62119-EL-HEL. The views expressed in this article are those of the author and do not reflect the official policy or position of the US government or the Department of Defense. Distribution A: Approved for public release, distribution unlimited.

References

1. B P Abbott et al 2009 Rep. Prog. Phys. **72** 076901 doi:10.1088/0034-4885/72/7/076901
2. Gregory D. Goodno, Lewis D. Book, and Joshua E. Rothenberg, Opt. Lett. **34**, 1204-1206 (2009).
3. N. Traynor, J. Boullet, R. Dubrasquet, S. Lugan, and G. Mery, in Advanced Photonics, OSA Technical Digest (online) (Optical Society of America, 2014), paper SoM3B.2.
4. Craig Robin, Iyad Dajani, and Benjamin Pulford, Opt. Lett. **39**, 666-669 (2014).
5. Chad G. Carlson, R. Brendan Ross, Jessica M. Schafer, Justin B. Spring, and Benjamin G. Ward, Phys. Rev. B **83**, 235110 (2011).
6. Arlee V. Smith and Jesse J. Smith, IEEE Journal of Selected Topics in Quantum Electronics vol. **20**, issue 5 (2014).
7. G. P. Agrawal, *Nonlinear Fiber Optics, 2nd Ed.* (Academic, 2001).
8. Kristian Rymann Hansen and Jesper Lægsgaard, Opt. Express **22**, 11267-11278 (2014).
9. B. G. Ward, Opt. Express **16**, 8532–8548 (2008).
10. B. G . Ward, Opt. Express **21**, 12053-12067 (2013).

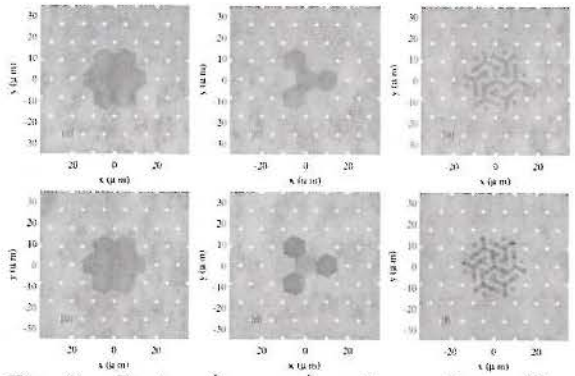

Fig. 6. Doping (top row) and acoustic profiles (bottom row) of a PCF (left), SAT (center) and μSAT (right) fibers. Darker shades of grey represent lower acoustic velocities whereas all doping concentrations are constant.

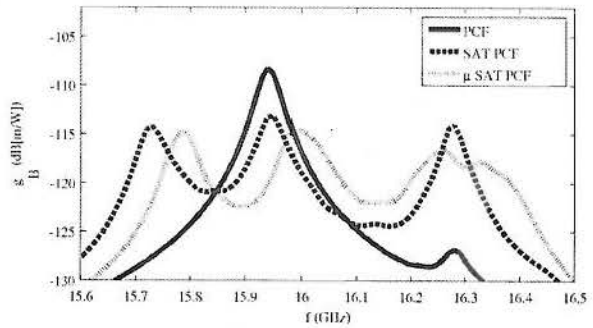

Fig. 5. Calculated Brillouin gain spectra of the three fibers

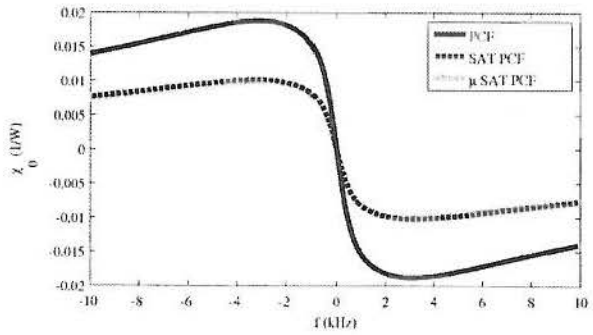

Fig. 4. Calculated mode coupling gain for the three fibers

References

1. B P Abbott et al 2009 Rep. Prog. Phys. **72** 076901 doi:10.1088/0034-4885/72/7/076901 LIGO: the Laser Interferometer Gravitational-Wave Observatory

2. Gregory D. Goodno, Lewis D. Book, and Joshua E. Rothenberg, "Low-phase-noise, single-frequency, single-mode 608 W thulium fiber amplifier," Opt. Lett. **34**, 1204-1206 (2009)

3. N. Traynor, J. Boullet, R. Dubrasquet, S. Lugan, and G. Mery, "Low-noise Single Frequency Fiber Lasers for Multi-watt Blue and Green Light Generation," in Advanced Photonics, OSA Technical Digest (online) (Optical Society of America, 2014), paper SoM3B.2.

4. Craig Robin, Iyad Dajani, and Benjamin Pulford, "Modal instability-suppressing, single-frequency photonic crystal fiber amplifier with 811 W output power," Opt. Lett. **39**, 666-669 (2014)

5. Chad G. Carlson, R. Brendan Ross, Jessica M. Schafer, Justin B. Spring, and Benjamin G. Ward, "Full vectorial analysis of Brillouin gain in random acoustically microstructured photonic crystal fibers," Phys. Rev. B **83**, 235110 (2011).

6. Arlee V. Smith and Jesse J. Smith, "Overview of a steady-periodic model of modal instability in fiber amplifiers," IEEE Journal of Selected Topics in Quantum Electronics vol. **20**, issue 5 (2014).

7. G. P. Agrawal, *Nonlinear Fiber Optics, 2nd Ed.* (Academic, 2001).

8. Kristian Rymann Hansen and Jesper Lægsgaard, "Impact of gain saturation on the mode instability threshold in high-power fiber amplifiers," Opt. Express **22**, 11267-11278 (2014)

9. B. G. Ward, "Bend performance-enhanced photonic crystal fibers with anisotropic numerical aperture," Opt. Express **16**, 8532–8548 (2008).

10. B. G . Ward, "Modeling of transient modal instability in fiber amplifiers," Opt. Express **21**, 12053-12067 (2013).